

Fig. 4. Cellulose-to-glucose conversion during saccharification of the senesced inflorescence stems of *cse* mutants. h, hours. Error bars indicate \pm SEM. * $0.05 > P > 0.01$, ** $0.01 > P > 0.001$, *** $0.001 > P$; unpaired two-sided *t* test.

convert *p*-coumarate to caffeate (24). However, these alternative routes to lignin biosynthesis do not fully compensate for a loss of CSE activity, because *cse* mutants are compromised in lignification and development. Likewise, the accumulation of caffeoyl shikimate that occurs in *cse* mutants suggests that HCT is relatively ineffective at metabolizing this substrate in vivo.

Lignin limits the processing of plant biomass to fermentable sugars (25, 26). Processing of *cse* mutant plants, which have reduced lignin content, might yield more sugars on saccharification. We compared cellulose-to-glucose conversion of senesced stems from both *cse* mutants and wild-type plants. Cell wall residues of senesced inflorescence stems of *cse-1* have normal amounts of cellulose, whereas those of *cse-2* have 73% of the normal amount of cellulose (table S2). The cellulose-to-glucose conversion of the untreated cell wall residue was monitored over a period of 48 hours (Fig. 4); when the plateau was reached, the conversion had increased from ~18% in the wild type to ~24% in *cse-1* (i.e., a relative increase of 32%) and to ~78% (fourfold higher than in the wild type) in *cse-2*. Therefore, saccharification efficiency increases as lignin content decreases. On a plant basis, *cse-2* mutants released 75% more glucose than the wild type. Saccharification efficiency from material derived from *cse-2* plants is similar to that of *ccr1-3*, a mutant in the lignin pathway gene for cinnamoyl-CoA reductase that has the highest saccharification efficiency described so far (26).

We found orthologs of CSE in a wide range of plant species (fig. S14), including biofuel feedstocks such as poplar, eucalyptus, and switchgrass. Consistent with a potential conserved role in lignification, CSE copurifies with lignin biosynthetic enzymes in extracts from poplar xylem

(27). The characterization of CSE in other species will reveal how widely the revision of the lignin biosynthetic pathway we propose here applies and whether CSE could be a generally useful target for reducing cell wall recalcitrance to digestion or industrial processing in biomass crops.

References and Notes

1. J. K. Weng, C. Chapple, *New Phytol.* **187**, 273–285 (2010).
2. F. Yang *et al.*, *Plant Biotechnol. J.* **11**, 325–335 (2013).
3. N. Mitsuda *et al.*, *Plant Cell* **19**, 270–280 (2007).
4. R. Zhong, E. A. Richardson, Z. H. Ye, *Planta* **225**, 1603–1611 (2007).
5. R. Vanholme *et al.*, *New Phytol.* **196**, 978–1000 (2012).
6. W. Boerjan, J. Ralph, M. Baucher, *Annu. Rev. Plant Biol.* **54**, 519–546 (2003).
7. R. Vanholme *et al.*, *Plant Cell* **24**, 3506–3529 (2012).
8. F. Chen *et al.*, *Plant J.* **48**, 113–124 (2006).
9. J. M. Humphreys, C. Chapple, *Curr. Opin. Plant Biol.* **5**, 224–229 (2002).
10. N. D. Bonawitz, C. Chapple, *Annu. Rev. Genet.* **44**, 337–363 (2010).
11. K. Freudenberg, A. C. Neish, in *Constitution and Biosynthesis of Lignin*, vol. 2 of *Molecular Biology, Biochemistry and Biophysics*, A. Kleinzeller, G. F. Springer, H. G. Wittman, Eds. (Springer-Verlag, New York, 1968), pp. 1–129.
12. J. Ralph *et al.*, *Phytochem. Rev.* **3**, 29–60 (2004).
13. G. Schoch *et al.*, *J. Biol. Chem.* **276**, 36566–36574 (2001).
14. R. Franke *et al.*, *Plant J.* **30**, 47–59 (2002).
15. R. Franke *et al.*, *Plant J.* **30**, 33–45 (2002).
16. L. Hoffmann, S. Maury, F. Martz, P. Geoffroy, M. Legrand, *J. Biol. Chem.* **278**, 95–103 (2003).
17. W. Gao, H. Y. Li, S. Xiao, M. L. Chye, *Plant J.* **62**, 989–1003 (2010).
18. S. R. Turner, C. R. Somerville, *Plant Cell* **9**, 689–701 (1997).
19. X. Li, N. D. Bonawitz, J.-K. Weng, C. Chapple, *Plant Cell* **22**, 1620–1632 (2010).
20. S. Besseau *et al.*, *Plant Cell* **19**, 148–162 (2007).
21. H. D. Coleman, J.-Y. Park, R. Nair, C. Chapple, S. D. Mansfield, *Proc. Natl. Acad. Sci. U.S.A.* **105**, 4501–4506 (2008).
22. J. Ehling *et al.*, *Plant J.* **19**, 9–20 (1999).
23. J. Raes, A. Rohde, J. H. Christensen, Y. Van de Peer, W. Boerjan, *Plant Physiol.* **133**, 1051–1071 (2003).
24. H.-C. Chen *et al.*, *Proc. Natl. Acad. Sci. U.S.A.* **108**, 21253–21258 (2011).
25. F. Chen, R. A. Dixon, *Nat. Biotechnol.* **25**, 759–761 (2007).

26. R. Van Acker *et al.*, *Biotechnology for Biofuels*, www.biotechnologyforbiofuels.com/content/6/1/46 (2013).
27. R. Nilsson *et al.*, *Mol. Cell. Proteomics* **9**, 368–387 (2010).

Acknowledgments: The authors thank A. Bleys for help in preparing the manuscript and K. Graham for technical support. We gratefully acknowledge funding through the European Commission's Directorate-General for Research within the 7th Framework Program (FP7/2007–2013) under grant agreements 211982 (RENEWALL) and 270089 (MULTIBIOPRO); Stanford University's Global Climate and Energy Project (Towards New Degradable Lignin Types, Novel Mutants Optimized for Lignin, Growth and Biofuel Production via Re-Mutagenesis, and Efficient Biomass Conversion: Delineating the Best Lignin Monomer-Substitutes); the Hercules program of Ghent University for the Synapt Q-ToF (grant AUG/014); the Bijzonder Onderzoeksfonds-Zware Apparatuur of Ghent University for the Fourier transform ion cyclotron resonance mass spectrometer (174PZA05); and the Multidisciplinary Research Partnership Biotechnology for a Sustainable Economy (01MRB510W) of Ghent University. R.V. is indebted to the Research Foundation-Flanders for a postdoctoral fellowship and L.S., I.C., and P.A. to the Agency for Innovation by Science and Technology (IWT), CAPES-Brazil (grant 201660/2010-5), and the CNPq-Brazil sandwich Ph.D. (grant 201998/2011-4), respectively, for predoctoral fellowships. J.R. and H.K. were funded in part by the U.S. Department of Energy's Great Lakes Bioenergy Research Center (DOE Office of Science BER DE-F02-07ER64494). G.G.S. was partially funded by the Scottish Government. W.B. is on the Science Advisory Board of the NSF-funded project Regulation and Modeling of Lignin Biosynthesis, DBI-0922391. A patent application, "Modified plants" PCT/GB2013/051206, on the modification of CSE expression to improve processes that require carbohydrate extraction, has been filed jointly by the University of Dundee and the Flanders Institute for Biotechnology (VIB).

Supplementary Materials

www.sciencemag.org/cgi/content/full/science.1241602/DC1
Materials and Methods
Figs. S1 to S14
Table S1 to S5
References (28–55)

7 June 2013; accepted 5 August 2013
Published online 15 August 2013;
10.1126/science.1241602

Epigenetic Regulation of Mouse Sex Determination by the Histone Demethylase Jmjd1a

Shunsuke Kuroki,¹ Shogo Matoba,² Mika Akiyoshi,¹ Yasuko Matsumura,¹ Hitoshi Miyachi,¹ Nathan Mise,^{2*} Kuniya Abe,² Atsuo Ogura,² Dagmar Wilhelm,^{3†} Peter Koopman,³ Masami Nozaki,⁴ Yoshiakira Kanai,⁵ Yoichi Shinkai,^{6‡} Makoto Tachibana^{1,7‡}

Developmental gene expression is defined through cross-talk between the function of transcription factors and epigenetic status, including histone modification. Although several transcription factors play crucial roles in mammalian sex determination, how epigenetic regulation contributes to this process remains unknown. We observed male-to-female sex reversal in mice lacking the H3K9 demethylase Jmjd1a and found that Jmjd1a regulates expression of the mammalian Y chromosome sex-determining gene *Sry*. Jmjd1a directly and positively controls *Sry* expression by regulating H3K9me2 marks. These studies reveal a pivotal role of histone demethylation in mammalian sex determination.

The development of two sexes is essential for the survival and evolution of most animal species. Although several transcrip-

tion factors, including the factor encoded by the Y chromosome gene *Sry* (1, 2), have been shown to play crucial roles in mammalian sex differen-

tiation, the contribution of epigenetic regulation to this process is largely unknown. *Sry* is required for male development (3), with sufficient and temporally accurate expression being critical for triggering the testis-determining pathway (4, 5).

Posttranslational modifications of histones are correlated with various chromatin functions, including control of gene expression. Among them, methylation of lysine 9 and lysine 4 of histone H3 (H3K9 and H3K4) are hallmarks of transcriptionally suppressed and activated chromatin, respectively (6). *Jmjd1a* (also called *Tsga/Jhdm2a/Kdm3a*), an enzyme that demethylates H3K9, is crucial for gene activation in spermiogenesis and metabolism (7–12).

¹Experimental Research Center for Infectious Diseases, Institute for Virus Research, Kyoto University, 53 Shogoin, Kawara-cho, Sakyo-ku, Kyoto, Japan. ²Bioresource Center, RIKEN Tsukuba Institute, 3-1-1 Koyadai, Tsukuba, Japan. ³Institute for Molecular Bioscience, The University of Queensland, Brisbane, Queensland 4072, Australia. ⁴Research Institute for Microbial Diseases, Osaka University, Suita, Osaka 565-0871, Japan. ⁵Department of Veterinary Anatomy, The University of Tokyo, Yayoi 1-1-1, Bunkyo-ku, Tokyo 113-8657, Japan. ⁶Cellular Memory Laboratory, RIKEN Advanced Science Institute, 2-1 Hirosawa, Wako-shi, Saitama 351-0198, Japan. ⁷Graduate School of Biostudies, Kyoto University, 53 Shogoin, Kawara-cho, Sakyo-ku, Kyoto, Japan.

*Present address: Department of Environmental Preventive Medicine, Jichi Medical University, 3311-1, Yakushiji, Shimotsuke, Tochigi, Japan.

†Present address: Department of Anatomy and Developmental Biology, Monash University, Clayton, VIC 3800, Australia.

‡Corresponding author. E-mail: yshinkai@riken.jp (Y.S.); mtachiba@virus.kyoto-u.ac.jp (M.T.)

When analyzing *Jmjd1a*-deficient (*Jmjd1a* Δ/Δ) mice, which had been established from C57BL/6 (B6) \times CBA F1 embryonic stem cells (11), we found that XY animals were frequently sex-reversed (table S1), either partially (12 of 58 animals) with a testis and an ovary (Fig. 1A) or completely (34 of 58 animals) with two ovaries (fig. S1). In contrast, all XY *Jmjd1a*^{+/+} and XY *Jmjd1a* Δ ⁺ mice had two testes (Fig. 1B and table S1). Notably, some of the completely sex-reversed animals were fertile (tables S1 and S2). The generation and comparison of XY *Jmjd1a*-deficient mice, carrying the Y chromosome from either CBA (Y^{CBA}) or B6 (Y^{B6}) on a B6 autosomal background (fig. S2), revealed that the sex-reversal phenotype was dependent on not only the loss of *Jmjd1a* but also the genetic origin of the Y chromosome combined with the B6 background. In total, 88% of XY^{CBA} but only 14% of XY^{B6} *Jmjd1a*-deficient mice displayed abnormal sex differentiation (Fig. 1B). Spermiogenesis defects were observed in XY^{CBA} as well as XY^{B6} *Jmjd1a*-deficient testes (fig. S1), as demonstrated previously (9, 12). XX *Jmjd1a*-deficient mice underwent normal sex differentiation and were fertile (table S1 and fig. S1).

To investigate the etiology of sex reversal, we examined expression of the testicular Sertoli cell marker *Sox9* (13) and the ovarian somatic cell marker *Foxl2* (14) in fetal gonads after sex determination at embryonic day 13.5 (E13.5) (Fig. 1C). XY *Jmjd1a*-deficient gonads contained both

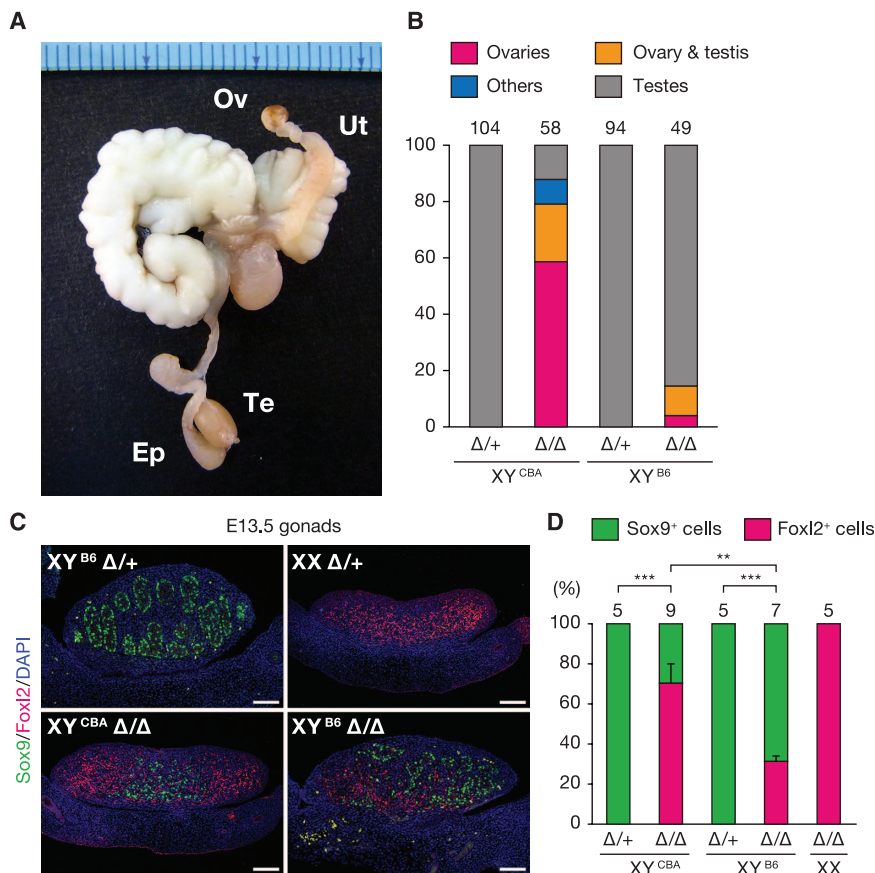
Sox9- and *Foxl2*-positive cells (Fig. 1D), indicative of ovotestes and therefore partial primary sex reversal, resulting from early failure of the testis-determining pathway. The number of *Sox9*-positive cells in XY^{B6} *Jmjd1a*-deficient gonads was higher than that in XY^{CBA}. This phenotypic difference was sustained even after the ninth generation of backcrossing to B6 (fig. S3).

To address the molecular basis of this phenotype, we determined the expression levels of *Sry* and its downstream target gene, *Sox9*. A quantitative real-time fluorescence polymerase chain reaction (RT-qPCR) analysis revealed that the *Sry* expression levels were reduced to approximately 30% in XY *Jmjd1a*-deficient gonads at E11.5 [corresponding to 17 to 19 tail somite (ts) stages (Fig. 2A)]. Expression of *Sry* was significantly lower in XY^{CBA}, as compared to XY^{B6}, in control and mutant gonads. It is conceivable that the *Sry* expression levels in *Jmjd1a*-deficient gonads at E11.5 might be near the threshold level for inducing the male pathway, and therefore the genetic background-dependent difference of *Sry* expression may critically affect the subsequent sexual development. *Sox9* expression was also reduced in XY *Jmjd1a*-deficient gonads (Fig. 2B).

A coimmunofluorescence analysis demonstrated that the number of *Sry*- and *Sox9*-positive cells was reduced to ~25% in XY *Jmjd1a*-deficient gonads at E11.5 (Fig. 2, C to F). The number of *Sry*-positive cells in XY^{CBA} gonads was slightly, but significantly, lower than that of XY^{B6} gonads

Fig. 1. *Jmjd1a*-deficient mice show XY sex reversal.

(A) Internal genitalia of partially sex-reversed XY *Jmjd1a*-deficient mice. Ov, ovary; Ut, uterus; Te, testis; Ep, epididymis. (B) Frequency analysis of abnormal sex differentiation between XY^{CBA} and XY^{B6} mice, determined by examining internal genitalia of adult mice. Genital classification is described in table S1 and fig. S1. Numbers of examined animals are shown above the bars. (C) Immunofluorescence analysis of E13.5 gonads. *Sox9* and *Foxl2* mark testicular Sertoli and ovarian somatic cells, respectively. Scale bar, 100 μ m. (D) Quantification of *Sox9*- and *Foxl2*-positive cells in E13.5 gonads. Numbers of examined embryos are shown above the bars. Data are presented as mean \pm SE. ***P* < 0.01; ****P* < 0.001 (Student's *t* test).



at E11.5 (fig. S4), presumably due to the different *Sry* mRNA amounts between them. On the other hand, the number of cells expressing Nr5a1, an orphan nuclear receptor expressed in gonadal somatic cells (15), was unchanged by *Jmjd1a* deficiency (fig. S5). A terminal deoxynucleotidyl transferase-mediated deoxyuridine triphosphate nick end labeling (TUNEL) assay and antibody to Ki67 immunostaining analysis demonstrated that *Jmjd1a* deficiency led to neither an increase in apoptosis nor a decrease in proliferation (fig. S6). In addition, we established a transgenic mouse line (LN#9) in which the gonadal somatic cells were specifically tagged with the cell surface marker protein CD271. The gonadal somatic cells were immunomagnetically isolated from these mice with high efficiency (fig. S7). Using these mice, we determined the numbers of gonadal somatic cells and found that control and mutant embryos contained similar numbers at E11.5 ($\sim 4 \times 10^4$ cells per gonad pair) (fig. S8), indicating that *Jmjd1a* deficiency did not affect gonadal somatic cell numbers. Thus, the critical role of Jmjd1a during mammalian sex determination is to ensure *Sry* expression above the threshold level.

To identify the critical step in the male sex-determining pathway that is controlled by Jmjd1a, we used two different approaches. First, we performed a microarray analysis to address whether *Jmjd1a* deficiency results in perturbed expression

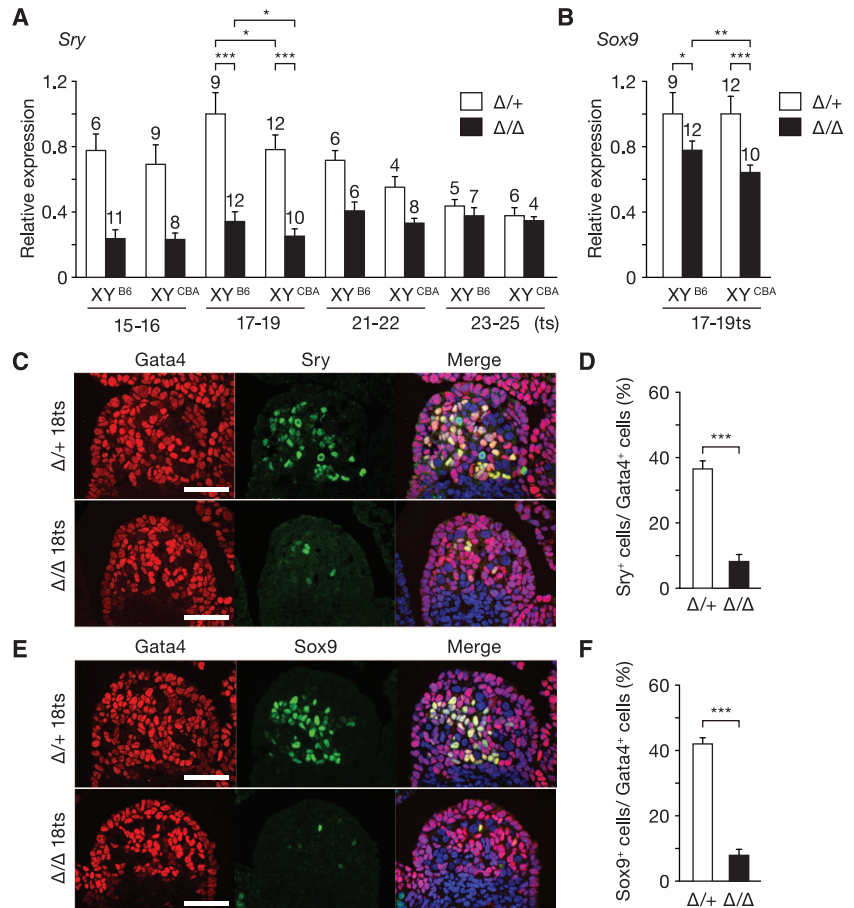
of known genes required for *Sry* expression. The analysis of a total of 41,181 probes revealed 131 genes, including *Sry*, with reduced (<0.5-fold) expression in XY *Jmjd1a* Δ/Δ , as compared to XY *Jmjd1a* $\Delta^+/+$ (table S3). However, *Jmjd1a* deficiency did not compromise expression of known *Sry* regulators (fig. S9), indicating that Jmjd1a contributes to a different mode of *Sry* regulation. Second, we attempted to rescue the mutant phenotype by experimentally restoring *Sry* function, by crossing the *Hsp-Sry* transgenic mouse line (16) into the *Jmjd1a*-deficient background. Forced expression of *Hsp-Sry* transgene rescued the defect of testis cord development in XY *Jmjd1a*-deficient gonads to the similar levels of those of XY control gonads (fig. S10). Furthermore, virtually no Foxl2-positive cells were observed in XY *Jmjd1a*-deficient gonads expressing the *Hsp-Sry* transgene (fig. S10), indicating that *Sry* acts epistatically to *Jmjd1a* in regulating male sex determination in mice.

We next investigated the expression profile of Jmjd1a protein during gonadal development. Jmjd1a was detected in gonadal somatic and germ cells but not in mesonephric cells at E11.5 (18 ts) (Fig. 3A). A comparative RT-qPCR analysis revealed that *Jmjd1a* was the most highly transcribed gene in E11.5 gonadal somatic cells, among those encoding enzymes involved in the maintenance of H3K9 methylation (fig. S11). An

RNA expression analysis indicated that the amount of *Jmjd1a* mRNA increased from E10.5 (8 to 10 ts) and reached a plateau around E11.5 in gonadal somatic cells (Fig. 3B). This temporal expression profile is consistent with direct regulation of *Sry* expression by Jmjd1a. An immunofluorescence analysis demonstrated that *Jmjd1a* deficiency resulted in an approximately two-fold increase in the signal intensities of H3K9me2 in gonadal cells at E11.5 (Fig. 3, C and D), indicating its substantial contribution to H3K9 demethylation. *Sry* expression is triggered in the center of XY gonads at around 12 ts (17, 18). We observed low levels of H3K9me2 throughout XY gonads at 12 ts (fig. S12), suggesting that Jmjd1a demethylates H3K9me2 before *Sry* expression. Abundant Jmjd1a expression and low levels of H3K9me2 were also observed in XX gonads at E11.5 (fig. S13).

To prove the direct link between Jmjd1a function and *Sry* expression, a chromatin immunoprecipitation (ChIP) analysis was performed, using purified gonadal somatic cells at E11.5. Jmjd1a was bound to regulatory regions within the *Sry* locus in wild-type cells (Fig. 4, A and B). *Jmjd1a* deficiency led to a significant increase in H3K9me2 levels within the *Sry* locus (Fig. 4C), without changing histone H3 occupancy (Fig. 4D). The H3K9me2 levels of the *Sry* locus were indistinguishable between XY^{B6} and XY^{CBA}

Fig. 2. *Jmjd1a* deficiency perturbs the expression of *Sry*. (A and B) RT-qPCR analyses of *Sry* (A) and *Sox9* (B) in XY gonads. Each of the samples included one pair of gonads/mesonephros. Results were normalized to *Gapdh*, and the expression levels in XY^{B6} *Jmjd1a* $\Delta^+/+$ were defined as 1. Numbers of examined embryos are shown above the bars. (C and E) Coimmunostaining profiles of *Sry* (C) and *Sox9* (E) with the gonadal somatic cell marker, *Gata4*, in XY^{CBA} gonads. (D and F) The ratios of the cells positive for *Sry* (D) and *Sox9* (F) to the cells positive for *Gata4*. Scale bar, 50 μ m. All data are presented as mean \pm SE. * $P < 0.05$; ** $P < 0.01$; *** $P < 0.001$ (Student's *t* test).



gonads at E11.5 (fig. S14), demonstrating the conserved role of *Jmjd1a* between these genetic backgrounds. The unchanged levels of H3K9me3 at the *Sry* locus, with or without *Jmjd1a*, indicated H3K9me2-specific demethylation by *Jmjd1a* (Fig. 4E). *Jmjd1a* deficiency resulted in perturbed H3K4 methylation of the *Sry* locus (Fig. 4F). In contrast to *Sry*, the H3K9me2 levels of *Sox9* were unchanged by *Jmjd1a* deficiency (fig. S15), indicat-

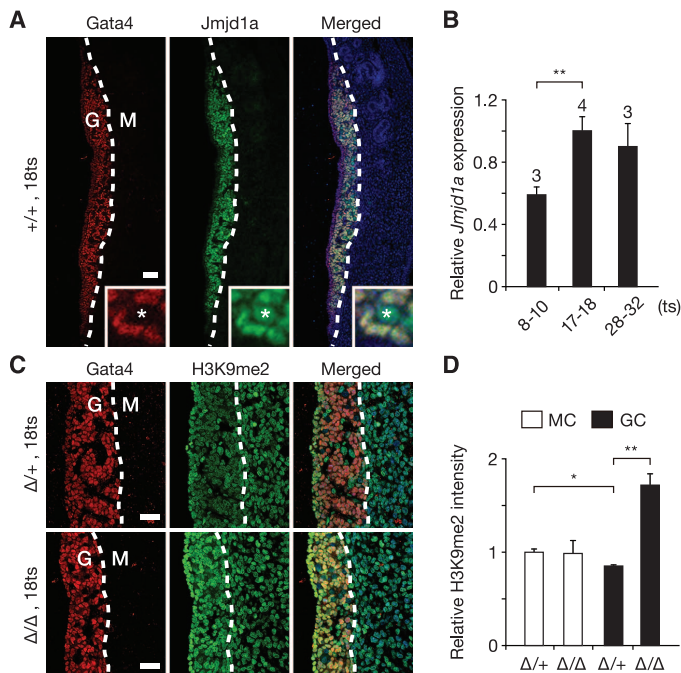
ing that *Jmjd1a* does not control *Sox9* expression directly. Coordinated H3K9 demethylation/H3K4 methylation was commonly observed in other *Jmjd1a* target genes (fig. S15), suggesting that *Jmjd1a*-mediated H3K9 demethylation is required for subsequent H3K4 methylation for transcriptional activation. Since *Sry* is located on the heterochromatic Y chromosome, *Jmjd1a*-mediated H3K9 demethylation may induce deheterochro-

matinization of *Sry*; to allow the access of the H3K4 methyltransferase and transcription factors (fig. S16).

This work shows a crucial role of a histone demethylase in *Sry* expression. Another chromatin regulator, Cbx2, reportedly plays a role in *Sry* expression in mice (19). However, in contrast to *Jmjd1a*, Cbx2 up-regulates the expression of several positive regulators of *Sry*, such as *Dax1*, *Gata4*, *Wt1*, and *Nr5a1* (19), suggesting that they might be involved in different phases of *Sry* expression. The discovery of the critical role of chromatin modification on *Sry* regulation not only provides new insights into the earliest steps of mammalian sex determination but also demonstrates the importance of epigenetic regulation in spatiotemporal gene regulation during embryonic development.

Fig. 3. *Jmjd1a* is expressed in developing gonads and catalyzes H3K9 demethylation.

(A) Coimmunostaining profiles of *Gata4* and *Jmjd1a* on sections of XY^{CBA} gonads. Enlarged box indicates that *Jmjd1a* signals were observed in gonadal somatic cells as well as germ cells (asterisks). G, gonad; M, mesonephros. Scale bar, 50 μm. (B) Quantitative analysis of *Jmjd1a* transcripts in purified gonadal somatic cells. Expression is normalized to *Gapdh*. Numbers of examined embryos are shown above the bars. (C) Coimmunostaining profiles of *Gata4* and H3K9me2 in XY^{CBA} gonads. G, gonad; M, mesonephros. Scale bar, 50 μm. (D) Quantitative comparison of the immunofluorescence intensities of H3K9me2 signals between gonadal and mesonephric cells. The intensities of H3K9me2 signals in *Jmjd1a*Δ⁺ mesonephric cells were defined as 1. MC, mesonephric cells; GC, gonadal cells. All data are presented as mean ± SE. *P < 0.05; **P < 0.01 (Student's *t* test).



References and Notes

1. R. Sekido, R. Lovell-Badge, *Trends Genet.* **25**, 19–29 (2009).
2. K. Kashimada, P. Koopman, *Development* **137**, 3921–3930 (2010).
3. P. Koopman, J. Gubbay, N. Vivian, P. Goodfellow, R. Lovell-Badge, *Nature* **351**, 117–121 (1991).
4. R. Hiramatsu *et al.*, *Development* **136**, 129–138 (2009).
5. D. Wilhelm *et al.*, *Mech. Dev.* **126**, 324–336 (2009).
6. S. M. Kooistra, K. Helin, *Nat. Rev. Mol. Cell Biol.* **13**, 297–311 (2012).
7. K. Yamane *et al.*, *Cell* **125**, 483–495 (2006).
8. M. Tachibana, M. Nozaki, N. Takeda, Y. Shinkai, *EMBO J.* **26**, 3346–3359 (2007).
9. Y. Okada, G. Scott, M. K. Ray, Y. Mishina, Y. Zhang, *Nature* **450**, 119–123 (2007).
10. K. Tateishi, Y. Okada, E. M. Kallin, Y. Zhang, *Nature* **458**, 757–761 (2009).
11. T. Inagaki *et al.*, *Genes Cells* **14**, 991–1001 (2009).
12. Z. Liu *et al.*, *J. Biol. Chem.* **285**, 2758–2770 (2010).
13. J. Kent, S. C. Wheatley, J. E. Andrews, A. H. Sinclair, P. Koopman, *Development* **122**, 2813–2822 (1996).
14. K. A. Loffler, D. Zarkower, P. Koopman, *Endocrinology* **144**, 3237–3243 (2003).
15. K. Morohashi, S. Honda, Y. Inomata, H. Handa, T. Omura, *J. Biol. Chem.* **267**, 17913–17919 (1992).
16. T. Kidokoro *et al.*, *Dev. Biol.* **278**, 511–525 (2005).
17. M. Bullejos, P. Koopman, *Dev. Dyn.* **221**, 201–205 (2001).
18. K. H. Albrecht, E. M. Eicher, *Dev. Biol.* **240**, 92–107 (2001).
19. Y. Katoh-Fukui *et al.*, *Endocrinology* **153**, 913–924 (2012).

Acknowledgments: We are especially grateful to T. Nakano for critical advice during the manuscript preparation. We thank K. Morohashi for antibodies to Nr5a1; H. Kimura for antibodies to histone; and T. Hara for fluorescence-activated cell sorting analysis support. We are also grateful to T. Matsui, G. Nagamatsu, and the members of the Tachibana laboratory for technical support. This work was supported by grants from the Funding Program for Next Generation World-Leading Researchers (M.T.). The microarray data have been deposited in the Gene Expression Omnibus and given the accession number GSE49513.

Supplementary Materials

www.sciencemag.org/cgi/content/full/341/6150/1106/DC1
Figs. S1 to S16
Tables S1 to S4
References (20–23)

30 April 2013; accepted 6 August 2013
10.1126/science.1239864

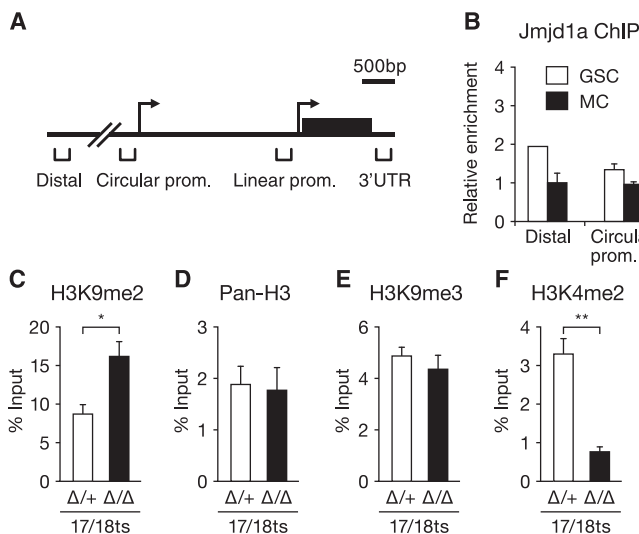


Fig. 4. *Jmjd1a* directly regulates H3K9 demethylation in the *Sry* locus. (A) Diagram of the *Sry* locus and the location of primer sets for ChIP-qPCR. (B) ChIP analysis with antibody to *Jmjd1a*, using purified XY^{CBA} gonadal somatic cells. GSC, gonadal somatic cells; MC, mesonephric cells. (C to

F) ChIP analysis for H3K9me2 (C), pan-H3 (D), H3K9me3 (E), and H3K4me2 (F) at the *Sry* linear promoter region of purified XY^{CBA} gonadal somatic cells. All data are presented as mean ± SE. *P < 0.05; **P < 0.01 (Student's *t* test).